# CHAPTER IV
# RESULTS AND DISCUSSION

## 4.1 Asphaltene Precipitation and Fractionation

Venezuela crude oil, which has 0.869 g/cm$^3$ in density (from weight measurement), was precipitated to yield asphaltene 7.54 wt % of crude oil. The yield of all asphaltene fractions are given in Figure 4.1. As can be seen from Figure 4.1, about half of the original asphaltene known as fraction 1 was obtained by precipitaing out using the ratio of pentane to $CH_2Cl_2$ of 70: 30. Fraction 1 was the most polar. It was also noticeable that approximately 14 wt % of the original asphaltenes did not precipitate out at 95:5 pentane:$CH_2Cl_2$. This might be due to the presence of small particles in the solution resulting in that the Brownian motion was dominant. These tiny particles, therefore, did not settle down in the solution eventhough the solution was centrifuged at 3,000 rpm in the given time of 30 minutes.

The solubility parameter of methylenedichloride is 7.1 dyne mol$^{1/3}$cm$^{-2}$ (9.8 cal$^{1/2}$ mol$^{1/2}$ cm$^{-3/2}$) while the solubility of asphaltene in pentane is 3.2 dyne mol$^{1/3}$cm$^{-2}$ (7.0 cal$^{1/2}$ mol$^{1/2}$ cm$^{-3/2}$). It is clearly noticed that the solvent power of $CH_2Cl_2$ is higher than that of pentane and is in the range of aromatic solvent which is considered as a good solvent to dissolve asphaltenes. Therefore, the solvent power of mixture of $CH_2Cl_2$ and n-pentane is decreased with decreasing the $CH_2Cl_2$ proportion from 30 vol % (the ratio of 30:70 $CH_2Cl_2$: n-pentane) to 5 vol % (the ratio 5:95 of $CH_2Cl_2$: n-pentane).

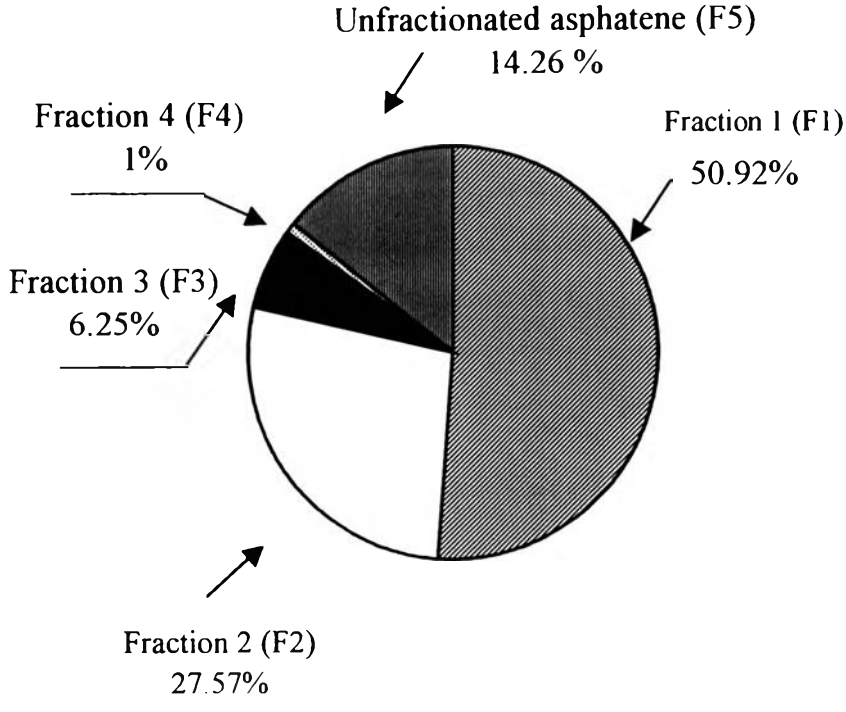


**Figure 4.1** Yield of asphaltene fractions as wt % of asphaltene originally dissolved in $CH_2Cl_2$.

According to the fact mentioned above, fraction 1 was considered being the most polar fraction as it precipitated in the solvent mixture, which had the highest solvent power. On the other hand, fraction 4 or residual asphaltene precipitates was considered as the least polar one. Polarity of fraction 2 and fraction 3 were in the between of fraction 1 and fraction 4.

## 4.2 Asphaltenes Characterization

### 4.2.1 Morphology Study

Figure 4.2 shows distinctions in morphology of fraction 1 and fraction 4. As can be seen from Figure 4.2, fraction 1 appears to have the large crystalline-like structure, which acts as a core and is covered with the sphere particles or the small size of clusters of the asphaltene particles. While each particle or cluster of fraction 4 branch out and loosely links particle by particle

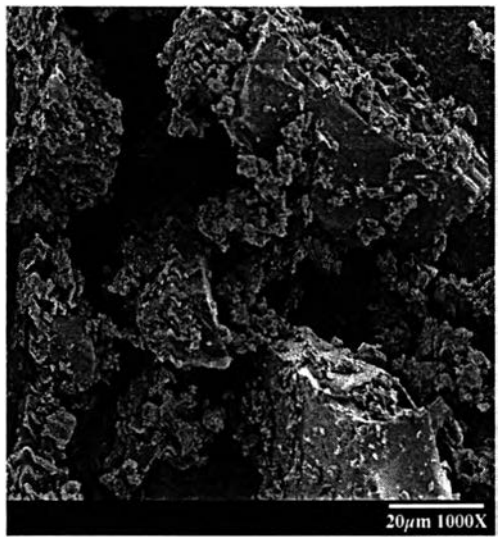


a) SEM picture of asphaltene F1 (1,000X)

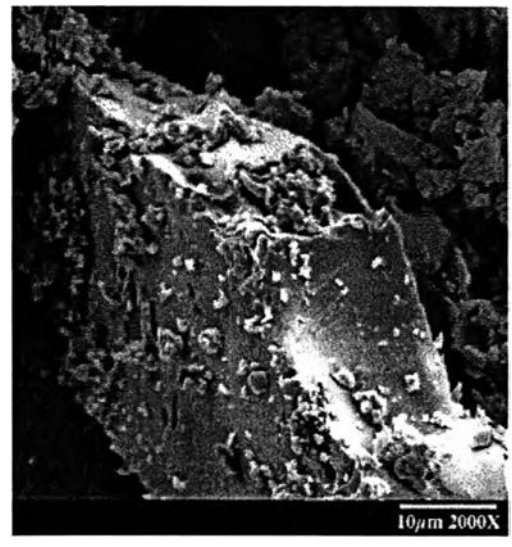


c) SEM picture of asphaltene F1 (1,000X)


b ) SEM picture of asphaltene F1 (2,000X)

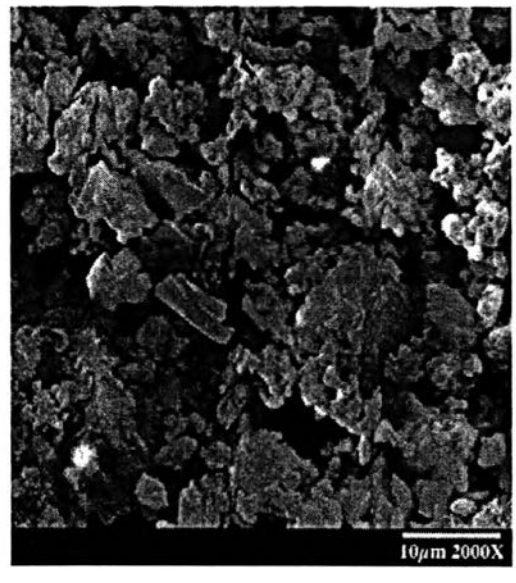


d) SEM picture of asphaltene F4 (2,000X)

**Figure 4.2** (a-d) SEM pictures of asphaltenes F1 and F4 at 1,000X and 2,000X in magnification.

(or cluster by cluster). It is very interesting to point out that the large crystal-like structure appeared in fraction 1 while the small and more porous structure presented in fraction 4. Consequently, the specific surface area and porosity of fraction 4 appeared higher than those of fraction 1.

It is known that asphaltene contains not merely aromatic compounds but also a variety of acidic and basic functional groups. Therefore, the large crystalline-like structure of asphaltenes appearing of the plat surface might result from the performing acid-base interaction as well as $\pi-\pi$ orbital association (Bunger and Yen, 1981). These interactions could occur among clusters as well as the individual charged particle of fraction 1 (the high polarity asphaltene). Moreover, the small clusters of particle which were the less polar asphaltene sticking on some specific sites on the surface might do coprecipitate with fraction 1. It might be explained this phenomenon that those specific sites stimulated adhering of the less polar particles or resin which might have the opposite charge in order to create electrical balance in the aggregates. On the other hand, fraction 4 showed significantly different from fraction 1. Another possible explanation is that the asphaltene fractions presenting in the different solvent mixtures have different flocculation models. (Muhammad et al., 1997).

4.2.2 Surface Areas of Asphaltenes

Table 4.1 shows the BET surface areas of the asphaltene samples. The BET surface areas of these three fractions show the progressive increase from fraction 1 to fraction 4. The measurement results agree very well with the SEM pictures of asphaltene fractions. The high porosity structure of fraction 4 resulted in the higher surface area and lower density.

**Table 4.1** BET surface areas of asphaltene fractions

| BET Surface area | F1 | F2 | F3 | F4 |
|---|---|---|---|---|
| ($m^2/g$) | 3.17 | - | 17.15 | 30 |

4.2.3 Elemental Composition of Asphaltenes

The elemental content (C, H, N, S) and metal content were reviewed in the Table 4.2 and Table 4.3, respectively. It is possible to obtain asphaltene fractions characterized, having different degree aromaticity and heteroatom content by using the fractionation method (Speight, 1980). The high degrees of aromaticity and heteroatom content should appear in the high polar fraction and the lower degrees of that should happen in the lower polar fraction. The heteroatomic chemical functions as well as organometallic compounds were often polar (Mullins, 1995). It is very interesting to point out that only the C/H ratio shown in table 4.2 gives a good corelation with the degree of aromaticity of asphaltene fractions. The C/H ratio decreased significantly from fraction 1 to fraction 4. However, the degree of aromaticity concluded from this technique is not accurate. The other techniques such as FT-IR and EA should be employed.

Surprisingly, the calculated value of oxygen content in the fraction 5 asphaltenes showed a minus sign which was not acceptable. This

**Table 4.2** Elemental composition of all asphaltene studied

| Fractions | C (wt.%) | H (wt.%) | N (wt.%) | S (wt.%) | O[1](wt.%) | C/H[2] |
|---|---|---|---|---|---|---|
| F0 | 85.615 | 7.993 | 1.457 | 4.044 | 0.891 | 0.893 |
| F1 | 85.595 | 7.501 | 1.656 | 3.914 | 1.334 | 0.951 |
| F2 | 85.950 | 7.595 | 1.593 | 3.361 | 1.501 | 0.943 |
| F3 | 85.451 | 7.840 | 1.726 | 3.167 | 1.816 | 0.908 |
| F4 | 83.231 | 7.808 | 1.562 | 3.417 | 3.982 | 0.888 |
| F5[3] | 85.679 | 10.630 | 0.393 | 6.046 | -2.750 | 0.672 |

1 oxygen content calculated from subtracting of all other contents

2 molar ratio

3 The unfractionated asphaltene in the F4's supernatant (Appendix A)

**Table 4.3** Metal contents in different asphaltene fractions

| Element | Units | Fraction 0* | Fraction 1 | Fraction 3 |
|---|---|---|---|---|
| Al | wt% | <0.01 | <0.01 | <0.01 |
| Ba | ppm | 20 | 10 | 20 |
| Be | ppm | <5 | <5 | <5 |
| Ca | wt% | <0.01 | <0.01 | 0.01 |
| Cd | ppm | <10 | <10 | <10 |
| Co | ppm | <10 | <10 | <10 |
| Cr | ppm | <10 | <10 | <10 |
| Cu | ppm | 10 | 10 | <10 |
| Fe | wt% | 0.02 | 0.03 | 0.01 |
| K | wt% | <0.01 | <0.01 | <0.01 |
| Mg | wt% | <0.01 | <0.01 | <0.01 |
| Mn | ppm | <10 | <10 | <10 |
| Ni | ppm | 260 | 330 | 260 |
| P | wt% | <0.01 | <0.01 | <0.01 |
| V | ppm | 1300 | 1600 | 1300 |
| Zn | ppm | 680 | 200 | 240 |

* The original asphaltene

invalid value value of oxygen content can be simply resulted from the atmospheric. Couples with the small quantities of oxygen in asphaltenes can also introduce uncertainty and impeded quantification of oxygen functional groups in asphaltene (Mullins, 1995).

Sulfur and nitrogen contents shown in Table 4.2 did not show any correlation with different asphaltene fractions. It might be resulted from the atmospheric oxidation could appear for sulfur-containing compound. Though, nitrogen fractions do not appear to be strongly altered (Mitra-Kirtly and Mullins, 1992). However, Mullins (1995) mentioned that it was unclear whether the sulfoxides were present in the asphaltenes before production of the corresponding crude oil or whether the sulfoxides resulted from air oxidation.

As can be seen from Table 4.3, Fe, V, Ni, and Zn called organometallic compounds are dominant in asphaltenes. One of the dominant organometallic components is porphyrin in nature as mentioned in Chapter 2. The structure of metalloporphyrin (metallated porphyrin) is depicted in Figure 4.3 (Saenger, 1984). The metalloporpyrin spectrum of zinc octaethylporphyrin compound (zinc OEP) had two distinct nitrogen types, pyrrolic and pyridinic nitrogen, with individual resonance structures (Saenger, 1984). Other metals containing in asphaltene (e.g. Fe, V, and Ni) may have the same structure as in Figure 4.3. However, these four metal ions might present in different organometallic nitrogen compounds. Moreover, these metals might present in pyrrollic or pyridinic components because both of them have the lone pair electron in $p_z$ and $sp^2$ orbital possible to bond with these metal ions. Surprisingly, the metal ions of Fe V, and Ni were rich in the polar fraction (fraction 1), but a significant amount of Zn was found in fraction 3, the less polar fraction. Zn ion might not prefer being in the form of metalloporphyrin structure normally present in the polar fraction, fraction 1, but it might prefer being in the form of other organometallic compounds instead.

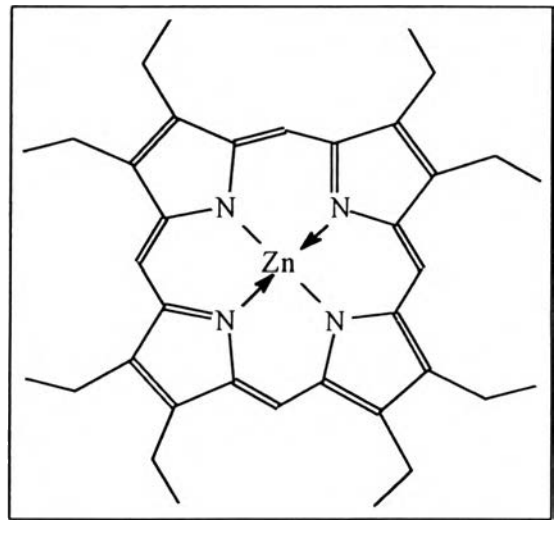


**Figure 4.3** Molecular structure of Zn–Metalloporphyrin interpreted from Nitrogen XANES spectrum (Saenger, 1984).

Functional groups containing oxygen, sulfur, nitrogen and several metal ions in the asphaltene structures are polar, so they tend to present in the more polar fraction. Figure 4.4 shows FT-TR spectrum of fraction 1, fraction 3, and the original asphaltene (F0). It can be seen from the FT-IR spectrum that the spectrum of the original asphaltene is significantly different from the one of fraction 1 and fraction 2, especially between 840 $cm^{-1}$-1340 $cm^{-1}$ wavenumber. Difference in intensity appeared between fraction 1 and fraction 3. The comparison of intensity/absorbance of a particular attenuation among them would be easier to differentiate these three types of asphaltene.

Table 4.4 gives IR band of all functional groups appearing in asphaltene fraction 1, fraction 3, and the original asphaltene. The oxygen-functional groups appeared at the low wavenumber (869-1261 $cm^{-1}$) and nitrogen-functional groups appear at the high wavenumber (3480 $cm^{-1}$). It is very interesting to point out that the amount of functional groups of fraction 1 are slightly less than that of fraction 3. It is the fact that the funtional groups are considered to be the polar part (positive or negative charges) in asphaltene molecule/structure. In addition, there are some functional groups, particularly nitrogen containing functional group, showing both basic and neutral in nature. Thus, it can be explained that the basic compound, which normally performs in the polar asphaltene, might prefer being in the less polar asphaltene.

From the FT-IR results, there is the highest intensity at 3480 $cm^{-1}$ even in the least polar fraction (fraction 3). It indicates that, N-H stretching detected might appear in different functional groups both in fraction 1 and fraction 3 since nitrogen containing functional groups can be basic in nature (polar functional group) and neutral (less polar functional group). It can be indicated that N-H presenting in fraction 1 results from polar functional group such as metalloporphyrinic structure. On the other hand, fraction 3 is largely possible to form other organic compounds, which have the less polar

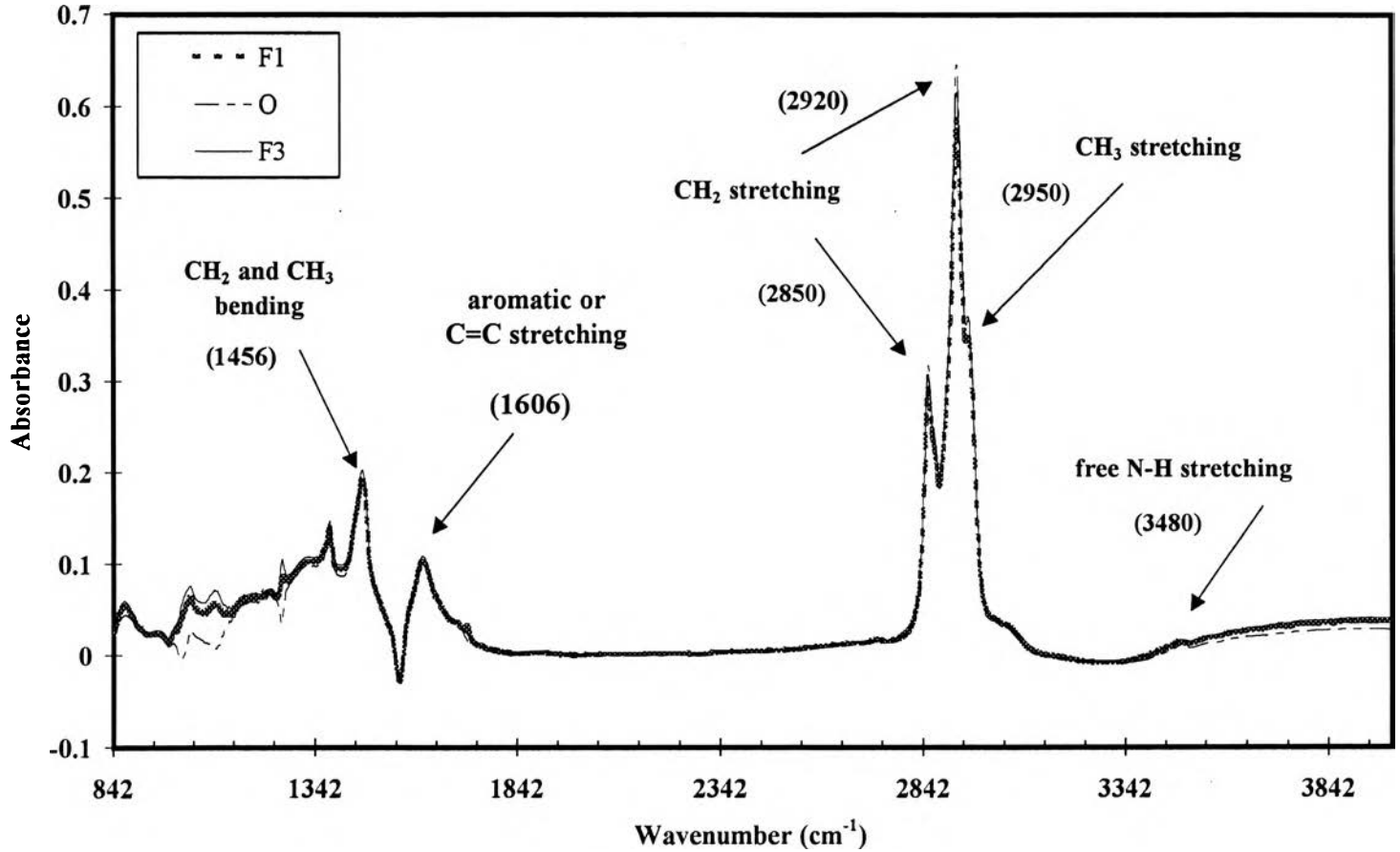


**Figure 4.4** FT-IR spectra of asphaltene fractions dissolved in $CCl_4$.

functional group (i.e., pyrrolic structure or porphyrenic compound (Saenger, 1984).

**Table 4.4** IR band absorbance appearing in asphaltene fractions

| Wavenumber ($cm^{-1}$) | Assignment | Absorbance | | |
|---|---|---|---|---|
| | | F0 | F1 | F3 |
| 3480 | Free N-H stretching | 0.01 | 0.014 | 0.017 |
| 3031(shoulder) | Aromatic C-H | 0.339 | 0.351 | 0.355 |
| 2954 | CH3 stretching | 0.371 | 0.349 | 0.366 |
| 2925 | Aliphatic-CH, ) | 0.654 | 0.587 | 0.625 |
| 2856 | CH2 and CH3 ) | 0.318 | 0.292 | 0.36 |
| 1606 | Aromatic of C=C stretching | 0.099 | 0.103 | 0.108 |
| 1456 | CH2 and CH3 bending | 0.195 | 0.191 | 0.201 |
| 1396 | CH3 group | 0.088 | 0.094 | 0.092 |
| 1261 | C-O stretching or C-H bending in phenoxy structures of ethers | 0.036 | 0.0874 | 0.105 |
| 1033 | Aliphatic ethers, alcohols | 0.01 | 0.056 | 0.071 |
| 869 | Isolated aromatic H | 0.044 | 0.054 | 0.059 |

At the low wavenumber (826-1261 $cm^{-1}$), oxygen functional groups in fraction 1 was lower intensity than in fraction 3. This unexpected result was probably due to the atmospheric oxidation during the fractionation experiment. The oxygen functional groups are the aliphatic ether, alcohol and C-O stretching/O-H bending in phenoxy structures as well as ethers.

## 4.3 Kinetic Dissolution of Asphaltenes

### 4.3.1 The Kinetic Dissolution of Asphaltene Fractions

The kinetics of asphaltene dissolution of different asphaltene fractions were studied. The apparent specific rate constants of asphaltene dissolution of the four asphaltene fractions were determined. Dodecylbenzene sulfonic acid (DBSA)/heptane binary solvent was used as dissolving media. The concentration of the binary solvent was fixed at 5 wt % of DBSA in heptane. The flow rate of this fluid was controlled at 1 ml/min. An experimental temperature was kept at 17 °C.

Figure 4.5 shows the time-evolution profile of asphaltene dissolution of the four different fractions. The results clearly showed that all fractions were effectively and completely dissolved by 5wt% of DBSA/heptane micellar fluid. The time for complete dissolving of asphaltene fraction 1 was relatively longer than that of asphaltene fraction 4. Figure 4.6 shows the plot of the logarithm of asphaltenene left in system ln (M/Mo) versus time). The apparent dissolution rate constant, $k_s$, was determined from the slope of linear fitting between ln (M/Mo) and time. However, the rate-limiting step was controlled by the surface reaction. Therefore, the rate of asphaltene dissolution should be generated by the rate of reaction. The asphaltene reaction rate ($k_r$, $g/m^2$-min) is derived from the specific rate constant ($k_s$, $min^{-1}$) divided by BET surface area. Both calculated values of $k_r$ and $k_s$ of asphaltene fractions are shown in Table 4.5. The $k_s$ value of asphaltenes fraction 1 and fraction 4 are 0.1823 $min^{-1}$ and 0.929 $min^{-1}$, respectively. It clearly showed that asphaltene fraction 4 was the easiest to be dissolved by the micellar fluid while asphaltene fraction 1 had the lowest dissolubilization. It is possible that asphaltene fraction 1 contained mostly large and robust aggregates, while asphaltene fraction 4 (see in Figure 4.2) was

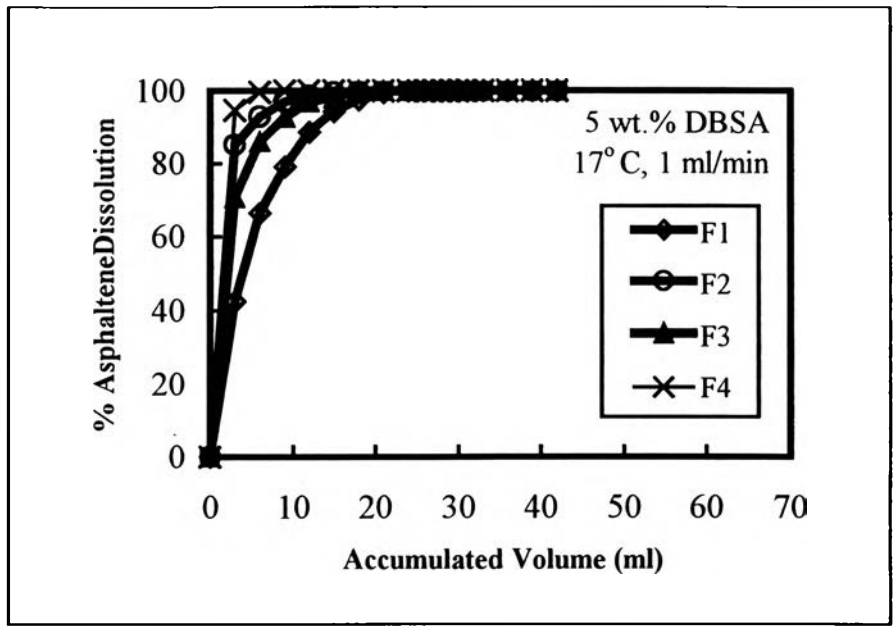


**Figure 4.5** The profile of asphaltene fractions dissolution by heptane-based fluid containing DBSA amphiphile.

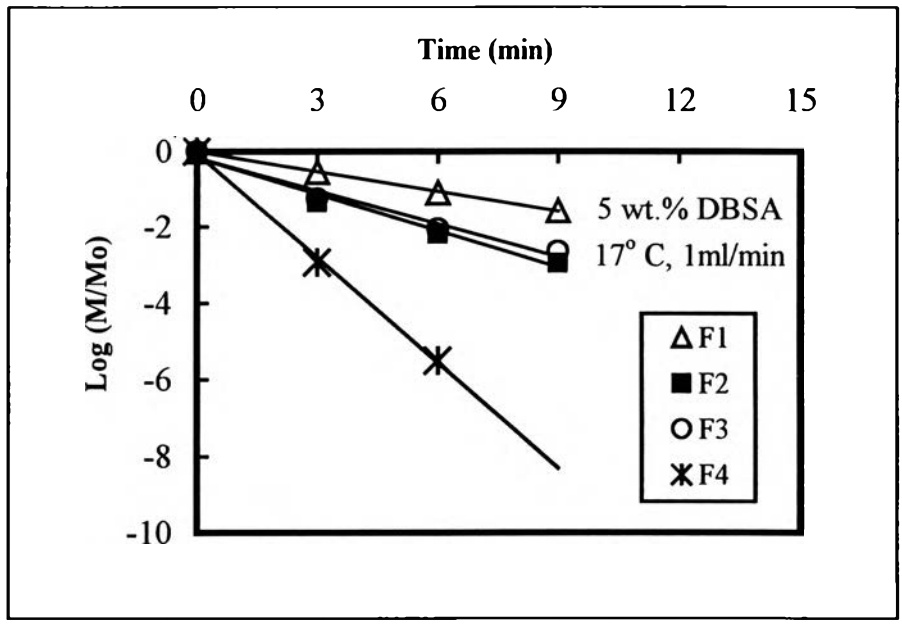


**Figure 4.6** Kinetic analysis of asphaltene fractions dissolution by heptane-based containing DBSA amphiphile.

more porous in structure. The higher surface area of asphaltene fraction 4 was dissolved easier than asphaltene fraction 1 having the lower surface area and large aggregate size. Oppositely, the reaction rate constant, $k_r$, of asphaltene fraction 1 (0.05751 $g/m^2$ x min) is clearly higher than that of asphaltene fraction 4 (0.03097 $g/m^2$ x min). This infers that a number of active sites with high energy appeared in asphaltene fraction 1. Therefore, if the surface area is not taken into consideration, asphaltene fraction 1 seems to be dissolved easier than fraction 4.

**Table 4.5** The dissolution rate constant of asphaltene fractions

| The dissolution rate constant | Asphaltene fractions | | | |
|---|---|---|---|---|
| | F1 | F2 | F3 | F4 |
| $k_s$ ($min^{-1}$) | 0.1823 | 0.3461 | 0.3153 | 0.929 |
| $k_r$ ($g/m^2$ min) | 0.05751 | - | 0.01838 | 0.03097 |

4.3.2 Effect of Amphiphile Concentration

The influence of the amphiphile concentration in the alkane based fluid on the apparent rate of asphaltene dissolution was carried out on asphaltenes fraction 1 and fraction 3 using dodecylbenzene sulfonic acid (DBSA)/heptane binary solvent (micellar fluid). The flow rate of fluid was fixed at 1 ml/min and the experiment temperature was maintained at 17 °C.

Figure 4.7 and Figure 4.8 show the time-evolution profile of asphaltene fraction 1 and fraction 3 dissolution as a function of DBSA concentration, respectively. Both figures show that effectiveness of asphaltene dissolution increases significantly with increasing the concentration of DBSA amphiphile. However, the trend of asphaltene dissolution with respect to DBSA concentration appeared quite different at concentrations of DBSA

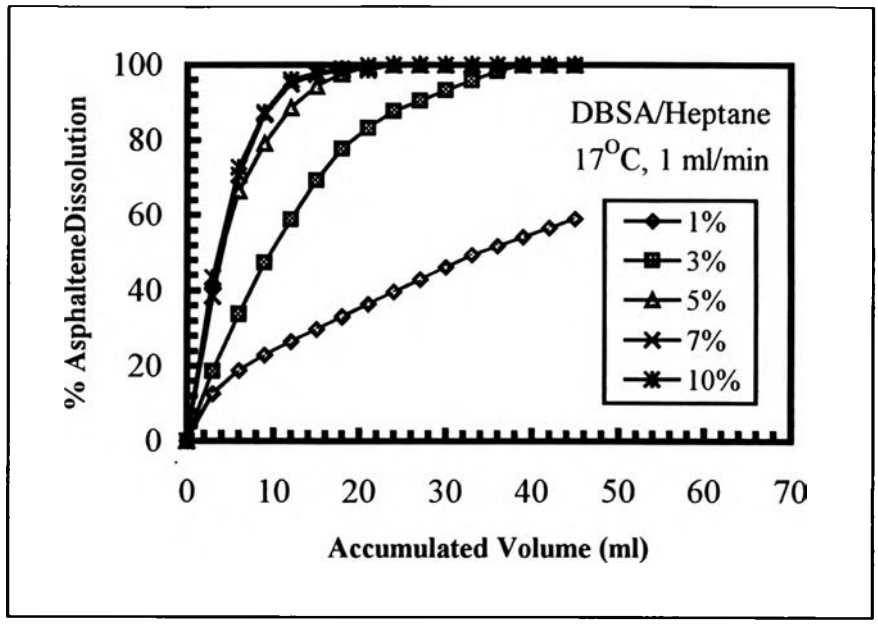


**Figure 4.7** The profile of asphaltene fraction 1 dissolution by heptane-based fluid containing different concentrations of DBSA amphiphile.

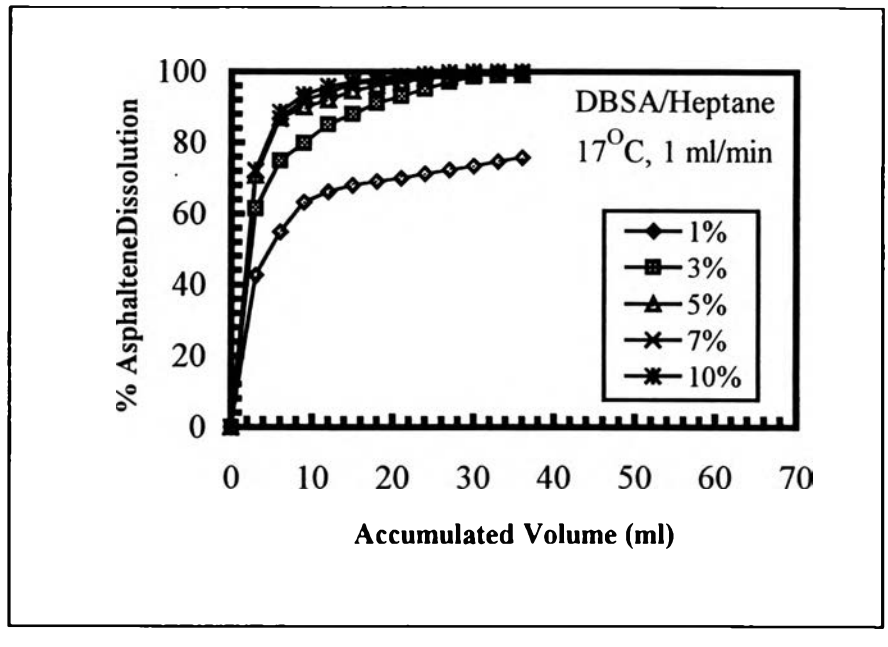


**Figure 4.8** The profile of asphaltene fraction 3 dissolution by heptane-based fluid containing different concentrations of DBSA amphiphile.

above and below 5 wt %. At the DBSA concentration less than 5 wt %, the asphaltene deposit was slowly dissolved while at the DBSA concentration greater than 5 wt %, the DBSA concentration did not affect the asphaltene dissolution profile both fraction a and fraction 3. It is noted that there is no difference in the minimum concentration required to completely dissolved asphaltene deposits. For both asphaltene fraction 1 and fractions 3, the minimum DBSA concentration wad approximately 3 wt%

Figures 4.9 and 4.10 show the plots of the logarithm of the undissolved asphaltene fraction (ln(M/Mo) versus time). The apparent dissolution rate constants of asphaltene fraction 1 and fraction 3 were calculated from the slopes of linear fitting between ln(M/Mo) and time. Table 4.6 gives the calculated values of the apparent specific rate constant ($k_s$) of asphaltene fraction 1 and fraction 3 at different concentrations of DBSA amphiphile. Figure 4.11 shows the plot between the apparent specific rate constant and DBSA concentration. Both asphaltene fraction 1 and fraction 3 had a similar trend. The apparent specific rate constant increased almost linearly with increasing the DBSA concentration when the DBSA concentration was below 0.11 M. When the DBSA concentration was greater than 0.11 M, the apparent specific rate constant leveled off. It can be seen clearly that the apparent specific rate of asphaltene fraction 3 was much higher than the value of fraction 1.

The apparent specific rate constant divided by BET surface area gives the reaction rate constant ($g/m^2 \times min$) showed in Table 4.7 and Figure 4.12. The reaction rate constants of both fraction 1 and fraction 3 increased almost linearly with increasing DBSA concentration. When the DBSA concentration was approximately 0.18 M, the reaction rate constant of both fractions leveled off. The maximum rate constants were 0.05751 ($g/m^2 \times min$) and 0.02076 ($g/m^2 \times min$) for fraction 1 and fraction 3, respectively. These

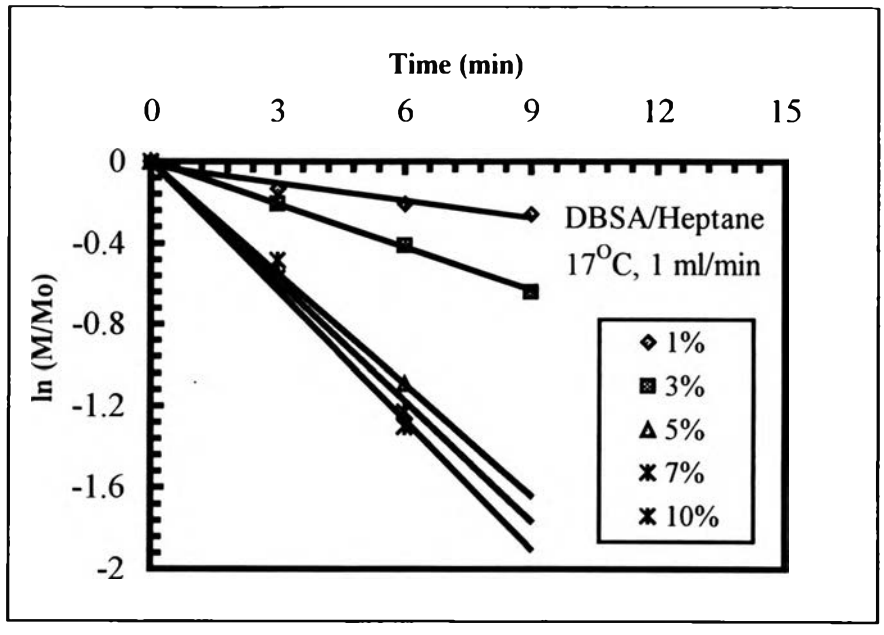


**Figure 4.9** Kinetic analysis of asphaltene fraction 1 dissolution by DBSA/heptane solutions containing different concentrations of DBSA amphiphile.

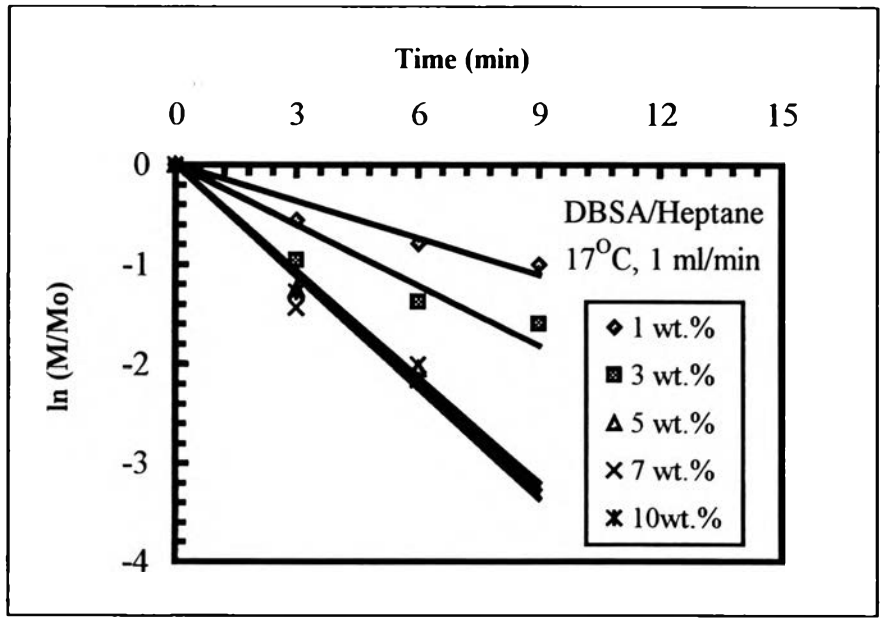


**Figure 4.10** Kinetic analysis of asphaltene fraction 3 dissolution by DBSA/heptane solutions containing different concentrations of DBSA amphiphile.

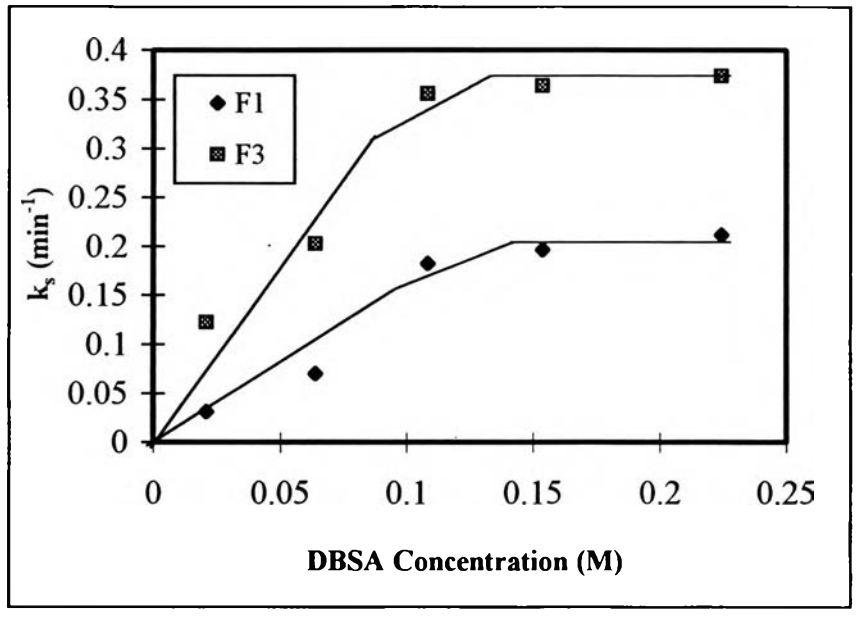


**Figure 4.11** The specific dissolution rate constant, $k_s$, as a function of DBSA concentraion in solutions.

**Table 4.6** The specific dissolution rate constant, $k_s$, for asphaltene fractions at different concentrations of DBSA amphiphile

| Concentration of DBSA amphiphile (M) | The specific dissolution rate constant, $k_s$ ($min^{-1}$) | |
|---|---|---|
| | Asphaltene fraction 1 | Asphaltenes fraction 3 |
| 0.0210 ( 1 wt%) | 0.0316 | 0.1226 |
| 0.0640 (3 wt%) | 0.0702 | 0.2025 |
| 0.1083 (5 wt%) | 0.1823 | 0.356 |
| 0.1538 (7 wt%) | 0.1961 | 0.3637 |
| 0.2245 ( 10 wt%) | 0.2114 | 0.3734 |

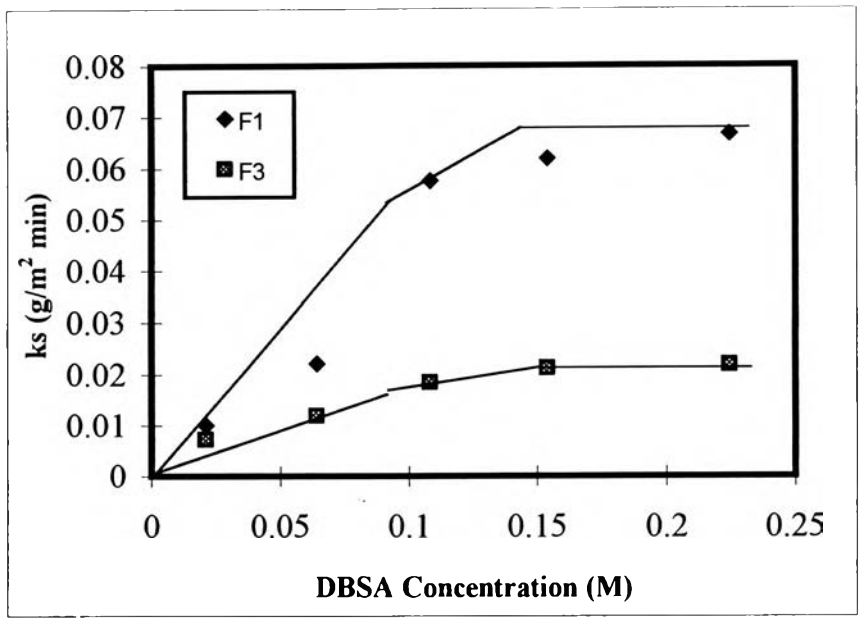


**Figure 4.12** The reaction dissolution rate constant of , $k_r$, as a function of DBSA concentraion in solutions.

**Table 4.7** Reaction rate constant, $k_r$, for asphaltene fractions at different concentrations of DBSA amphiphile

| Concentration of DBSA amphiphile (M) | The reaction rate constant, $k_r$ ($g/m^2$-$min^{-1}$) | |
|---|---|---|
| | Asphaltene fraction 1 | Asphaltenes fraction 3 |
| 0.0210 (1 wt%) | 0.0100 | 0.0071 |
| 0.0640 (3 wt%) | 0.0221 | 0.0118 |
| 0.1083 (5 wt%) | 0.0575 | 0.0208 |
| 0.1538 (7 wt%) | 0.0619 | 0.0212 |
| 0.2245 (10 wt%) | 0.0667 | 0.0218 |

trends suggest that the variation of $k_r$ with respect to the amphiphile concentration can be described by Langmuir-Hinshelwood kinetics.

The dissolution of asphaltene precipitates in amphiphile/alkane solution involves both mass transfer and surface reaction processes (Fogler, 1992). As a result of ICP technique, metals in the form of porphyrin structure showed considerable difference between fraction 1 and fraction 3. It could be hypothesized that metals play in an important role in the kinetics dissolution. Consequently, in order to stabilize asphaltene molecule, two molecules of DBSA are needed. The rate of asphaltene could be rederived.

When the amphiphiles absorb on the functional sites (metalloporphyrin compound) on the asphaltene surface,

$$A + 2S_{sf} \underset{k_{-A}}{\overset{k_A}{\rightleftharpoons}} A\bullet 2S_{sf} \qquad (4.1)$$

To form the amphiphile - asphaltene complex

$$A\bullet 2S_{sf} \xrightarrow{k_r} (A\bullet 2S)sf^{*} \qquad (4.2)$$

The rate of asphaltene dissolution varied with amphiphile concentration indicates that the surface reaction between asphaltene and amphiphile can be expressed as an equilibrium reaction.

The total number of functional sites on asphaltene surface is assumed to be proportional to the mass of undissolved asphaltenes and is the sum of bound and unbound sites. That is,

$$M = A + (A \bullet 2S_{sf}) = [A] + K_A[A]\left[S_{sf}^2\right]$$
$$[A] = \frac{M}{1 + K_A\left[S_{sf}^2\right]} \qquad (4.3)$$

The rate of asphaltene dissolution becomes

$$-\frac{dM}{dt} = k_r\left[A \bullet 2S_{sf}\right] = k_r K_A \frac{M\left[S_{sf}^2\right]}{1 + K_A\left[S_{sf}^2\right]} \qquad (4.4)$$

At very low DBSA concentration, the rate of asphaltenes dissolution exponentially increase with increasing DBSA concentration and level off at high DBSA concentration.

As can be seen in Figure 4.11 or Figure 4.12, at very low amphiphile concentration (lower 0.1 M), the rate of the amount of amphiphile adsorbing on asphaltene surface increases exponentially with increasing the concentration of amphiphile. At sufficiently high amphiphile (higher than 0.1 M), most of functional groups (active sites) on asphaltene surfaces have been already bonded with amphiphiles. Thereby, the rate of asphaltene dissolution cannot further increase with increasing the amphilphile concentration.

## 4.4 Acid-Base Interaction Study

Chang and Fogler (1994) found that an absorbance of a free SO-H stretching band appeared at the wavelength of 1800-2800 $cm^{-1}$. A decrease in the SO-H stretching band happened in the presence of asphaltene. This decrease can be due to the breakage of SO-H streching of DBSA. A proton of sulfonic group is able to irreversibly transfer to the corresponding conjugate basic groups on asphaltenes. Therefore, in this study, the acid-base interaction of asphaltene fraction 1 and fraction 3 was investigated by considering the SO-H streching band. Figure 4.13 shows a lower absorbance of the free SO-H stretching band in fraction 1 than that in fraction 3. This refers that the corresponding conjugate basic group presenting in fraction 1 was possibly more than fraction3 (Chang and Fogler, 1994). In other words, the sulfonic

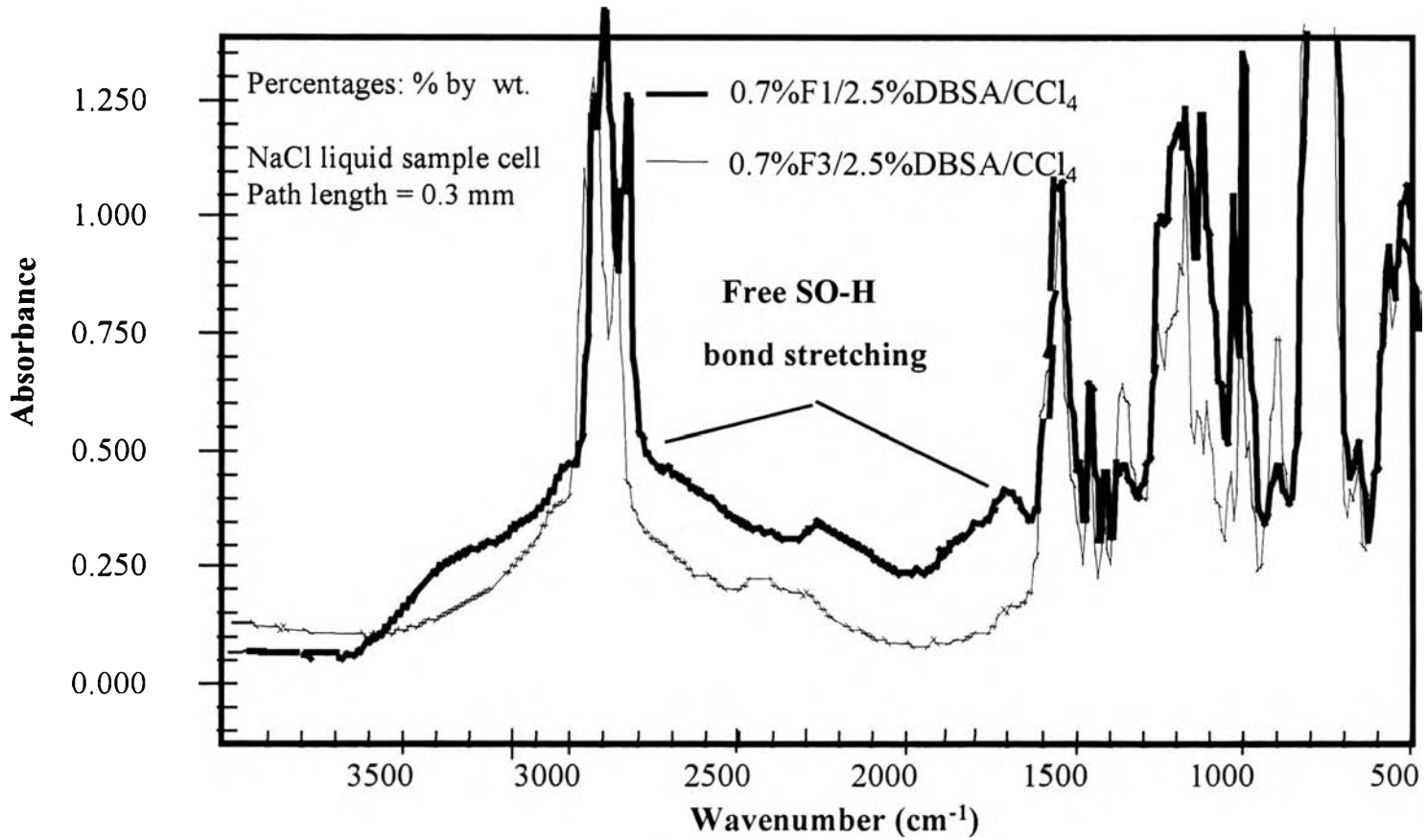


**Figure 4.13** FTIR spectra band showing amphiphile-asphaltene interaction of two Asphaltene fraction 1 and fraction 3.

groups might be consumed by the presence of the extremely active sites. Possibly, asphaltene fraction 1 contained active sites in greater amount than asphaltene fraction 3.

Moreover, it is possible that the activation energy of active sites of fraction 1 was relatively lower than fraction 3. Consequently, the reaction rate constant of fraction 1 appeared to be higher that of than fraction 3.